

Submitted to the Astrophysical Journal

## Dynamics of the Solar Magnetic Network Two-dimensional MHD Simulations

S. S. Hasan

*Indian Institute of Astrophysics, Bangalore-560034, India (hasan@iiap.res.in)*

A. A. van Ballegoijen and W. Kalkofen

*Harvard-Smithsonian Center for Astrophysics, 60 Garden Street, Cambridge, MA 02138,  
U.S.A.*

and

O. Steiner, Kiepenheuer Institut für Sonnenphysik, 7800 Freiburg, Germany

### ABSTRACT

The aim of this work is to identify the physical processes that occur in the network and contribute to its dynamics and heating. We model the network as consisting of individual flux tubes with a non-potential field structure that are located in intergranular lanes. With a typical horizontal size of 200 km at the base of the photosphere, they expand upward and merge with their neighbors at a height of about 600 km. Above a height of approximately 1000 km the magnetic field starts to become uniform.

Waves are generated in this medium by means of motions at the lower boundary. We focus on transverse driving, which generates both fast and slow waves within a flux tube and acoustic waves at the interface of the tube and the field-free medium. The acoustic waves at the interface are due to compression of the gas on one side of the flux tube and expansion on the other. These waves travel upward along the two sides of the (2D) flux tube and enter it, where they become longitudinal waves. For impulsive excitation with a time constant of 120 s, we find that a dominant feature is the creation of vortical motions that propagate upward. We have identified an efficient mechanism for the generation of longitudinal waves and shock formation in the chromospheric part of the flux concentration. We examine some broad implications of our results.

*Subject headings:* MHD — Sun: chromosphere — Sun: magnetic fields — Sun: oscillations

## 1. Introduction

The quiet solar chromosphere is bifurcated into the magnetic network on the boundary of supergranulation cells and the largely field-free internetwork medium in the cell interior, with respective filling factors in the ratio of 2 to 3 in the middle chromosphere (i.e., at a height of about 1 Mm above the level of unit optical depth at 5,000 Å). The network is about 30% brighter in Ca II K<sub>2v</sub> emission than the internetwork chromosphere (Skumanich, Smythe & Frazier 1975). Both the network and the internetwork medium show *bright points* (BPs), which are prominent in the emission peaks in the cores of the Ca II H and K lines, formed in the middle chromosphere. However, the dynamical and spectral properties of network and internetwork BPs are quite different. In internetwork areas the chromospheric velocity power spectrum is dominated by oscillations with frequencies at and above the acoustic cutoff frequency (period 3 min in upper photosphere, e.g., Rutten & Uitenbroek 1991), whereas in the network, Ca II H line center velocity and intensity power spectra are dominated by low-frequency oscillations with periods of 7-20 min (Lites, Rutten & Kalkofen 1993). These long-period waves have also been observed at larger heights (Curdt & Heinzel 1998; McAteer et al. 2002, 2003). Furthermore, network BPs show high emission in the line core most of the time (Lites et al. 1993), whereas internetwork locations have a bright phase only about 5% to 10 % of the time (von Uexküll & Kneer 1995). Finally, 80% of network BPs have symmetric profiles in the line core, with more or less equal intensity in the blue and red emission peaks on either side of the central absorption. In contrast, only about 30% of internetwork BPs have symmetric profiles, and 40% have blue-peak enhancements (Grossmann-Doerth, Kneer & v.Uexküll 1974); hence the name H<sub>2v</sub> or K<sub>2v</sub> bright point.

While the qualitative properties of internetwork BPs are reasonably well understood, including their formation in upward-propagating acoustic shocks that encounter downward-flowing gas (Carlsson & Stein 1995), this is not true for network BPs. The physical processes that heat the magnetic network have not been fully identified. Are network BPs heated by wave dissipation, and if so, what is the nature of these waves? How can we understand the observed relatively constant emission and symmetric line profiles of network BPs? The source of energy for network BPs is likely to be magnetohydrodynamic waves. Possible candidates are:

- Kink (transverse) waves, generated inside flux tubes by the buffeting action of granules;
- Longitudinal waves, generated by pressure fluctuations inside flux tubes;
- Torsional (Alfvén) waves, generated inside flux tubes;
- acoustic waves, generated in the field-free atmosphere surrounding flux tubes, that

penetrate into the tubes;

- Acoustic waves, generated at the interface of flux tubes and the outside medium, that also penetrate into the flux tubes.

The first three are well-known flux tube modes (e.g., Spruit 1981). Several investigations have focused on the generation and propagation of transverse and longitudinal wave modes and their dissipation in the chromosphere (e.g., Zhugzhda, Bromm & Ulmschneider 1995; Fawzy et al. 2002; Ulmschneider 2003 and references therein). Torsional waves have received some attention (e.g., Hollweg 1982; Noble, Musielak & Ulmschneider 2003). The fourth wave type is an obvious source since it is responsible for heating the internetwork medium. However, the importance of the fifth wave type, which we found during the course of this investigation, does not appear to have been adequately recognized earlier. It will be discussed in more detail later on.

The present study is a continuation of earlier work on the excitation of transverse and longitudinal waves in magnetic flux tubes by the impact of fast granules on flux tubes (Hasan & Kalkofen 1999), as observed by Muller & Roudier (1992) and Muller et al. (1994), and following the investigation by Choudhuri, Auffret & Priest (1993), who studied the generation of kink waves by footpoint motion of flux tubes. The observational signature of the modeled process was highly intermittent in radiation emerging in the H and K lines, contrary to observations. By adding waves that were generated by high-frequency motion due to the turbulence of the medium surrounding flux tubes (Hasan, Kalkofen & van Ballegooijen 2000), the energy injection into the gas inside a flux tube became less intermittent, and the time variation of the emergent radiation was in better agreement with the more steady observed intensity from the magnetic network.

The above studies modeled wave excitation and propagation in terms of the Klein-Gordon equation, motivated by the identification of the power peak near 7 min in the observed power spectrum (Lites et al. 1993; Curdt & Heinzel 1998; McAteer et al. 2002) with the cutoff period of kink waves in thin magnetic flux tubes (Kalkofen 1997). This analysis was based on a linear approximation in which the longitudinal and transverse waves are decoupled. However, it is well known that the velocity amplitude  $v(z)$  for the two modes increases with height  $z$  (for an isothermal atmosphere, as  $v \propto \exp[z/4H]$ , where  $H$  is the pressure scale height), so that the motions are expected to become supersonic higher up in the atmosphere. At such heights, nonlinear effects become important, leading to a coupling between the transverse and longitudinal modes. Some progress on this question has been made in one dimension, using the nonlinear equations for a thin flux tube, by Ulmschneider, Zähringer & Musielak (1991), Huang, Musielak & Ulmschneider (1995), and Zhugzhda,

Bromm & Ulmschneider (1995), and more recently by Hasan et al. (2003) and Hasan & Ulmschneider (2004), who examined mode coupling between transverse and longitudinal modes in the magnetic network. By solving the nonlinear, time-dependent MHD equations it was found that significant longitudinal wave generation occurs in the photosphere, typically for Mach numbers as low as 0.2, and that the onset of shock formation occurs at heights of about 600 km above the photospheric base, accompanied by heating (Hasan et al. 2003, Hasan & Ulmschneider 2004). The efficiency of mode coupling was found to depend on the magnetic field strength in the network and is a maximum for field strengths corresponding to  $\beta \approx 0.2$ , when the kink and tube wave speeds are almost identical. This can have interesting observational implications. Furthermore, even when the two speeds are different, once shock formation occurs, the longitudinal and transverse shocks exhibit strong mode coupling.

The above studies on the magnetic network make use of two important idealizations: they assume that the magnetic flux tubes are thin, an approximation that becomes invalid at about the height of formation of the emission peaks in the cores of the H and K lines; and they neglect the interaction of neighboring flux tubes. Some progress in this direction has recently been made by Rosenthal et al. (2002) and Bogdan et al. (2003), who studied wave propagation in a two-dimensional stratified atmosphere, assuming a potential magnetic field to model the network and internetwork regions on the Sun. They examined the propagation of waves that are excited from a spatially localized source in the photosphere. Their results indicate that there is strong mode coupling between fast and slow waves at the so-called magnetic canopy, which they identify with regions where the magnetic and gas pressures are comparable. As a consequence of the potential-field approximation, some magnetic field lines are nearly horizontal even at the base of the field. Such a model may not be appropriate for a network patch, which is perhaps better idealized as a collection of vertical tubes (Cranmer & van Ballegoijen 2005).

Thus the problem that we address concerns wave propagation in regions that are largely representative of individual structures in the magnetic network — this is different from the one analysed by Rosenthal et al. and Bogdan et al. Our initial configuration consists of flux tubes in 2-D magnetostatic equilibrium with a sharp interface between the tube and the surrounding gas. Waves are generated in this medium by means of transverse motion at the lower boundary, which displaces the entire flux tube, unlike the problem studied in the above papers where the source region is confined to a portion of the magnetic structure. This can have interesting consequences, some of which were unrecognized thus far. These will be explored in later sections of the paper. Our calculations indicate the presence of a new and efficient mechanism for longitudinal wave generation and shock formation in the chromosphere.

The present study forms the first of a series devoted to a detailed investigation of wave propagation in the magnetic network. As a first step, we go beyond the thin flux tube approximation and employ a two-dimensional treatment in slab geometry, similar to Rosenthal et al. and Bogdan et al. It is not possible (within the 2-D framework) to examine kink and sausage waves, which would require a three-dimensional treatment, but, nevertheless, there are still many important physical effects that this approach allows us to examine. For simplicity, we neglect non-adiabatic effects at this stage, which we will include in a separate paper.

Several papers have looked at MHD waves in various geometries in the solar atmosphere using multi-dimensional simulations (e.g., Shibata 1983; Cargill, Spicer, & Zalesak 1997; Ofman & Davila 1998; Sakai, Igrarashi & Kawata 1998; Ofman, Nakariakov, & DeForest 1999; additional references can be found in Bogdan et al. 2003).

The organization of this paper is as follows: in Sect. 2 we describe the initial equilibrium model, its construction and in Sect. 3 the numerical method of solution along with the driving mechanism. The results of our calculation are presented in Sect. 4 followed by a discussion and summary in Sect. 5.

## 2. Model

Following Cranmer & van Ballegoijen (2005), we treat a network element (typical flux  $\sim 3 \times 10^{19}$  Mx) to consist of a collection of smaller flux tubes that are spatially separated from one another in the photosphere. The gas pressure in the atmosphere decreases with increasing height, causing a lateral expansion of the flux tubes. Neighboring flux tubes within the network element merge into a monolithic structure at some height. Above this “merging height” the network element consists of a single thick flux tube that further expands with height. The outer edge of this tube forms a magnetic canopy that overlies the neighboring supergranular cells. A second merging occurs when neighboring network elements come together at a canopy height. Figure 1 schematically shows the picture we have for the network field structure. It consists of three distinct regions:

1. Photospheric region up to about 0.6 Mm, consisting of individual flux tubes, with a typical diameter of 200 km in the low photosphere. Their foot points are located in intergranular lanes and separated from one another by about the diameter of a granule ( $\sim 1$  Mm). They expand upward and merge with their neighbors at a height of about 0.6 Mm.
2. Lower chromosphere, between the heights of 0.6 and 1 Mm, the merged network flux

element expands laterally over the surrounding supergranular cell-center and overlying field-free chromosphere;

3. Upper chromosphere and corona, between 1 and 12 Mm, the fully merged magnetic field fills the available volume. At larger heights, the field expands primarily in the vertical direction and becomes more or less uniform. However, at lower heights, between 1 and 2 Mm, the field strength varies significantly with horizontal position, and the field strength directly above the flux tubes (left side of Figure 1) is much larger than above the supergranular cell center (right side of Figure 1).

Our model is based on the idea that the base of flux tubes is located in subsurface layers where convective flows may be different from those in the visible photosphere. Flux tubes occur in regions with convective downflows below intergranular lanes. These downflows are likely to be highly turbulent, involving lateral motions that produce transverse waves in the flux tubes. When the upward propagating waves reach the photosphere, they cause horizontal motions of flux tubes relative to their local surroundings. This generates excess pressure on the leading edge of a flux tube, and a pressure deficit on the trailing edge. Our two-dimensional MHD calculations (see section Sect. 3) indicate that these pressure pulses produce an upward-velocity pulse on the leading side of the flux tube and a downward pulse on the trailing side. These pressure pulses and vertical flows are an integral part of the MHD wave, so the transverse and longitudinal motions are strongly coupled.

### 2.1. Initial Two-dimensional Magnetostatic Model

Let us consider an individual flux tube at the base of a magnetic network element on the quiet sun; the region of interest is indicated by the small box in Figure 1. At heights below about 600 km, the flux tubes are spatially distinct from one another, and are embedded in a field-free “external” medium. At  $\approx 1000$  km, the flux tubes merge into a more uniform field (upper part of small box). The structure of the flux tube at the initial instant is assumed to be in static equilibrium and is determined by the magnetostatic force balance equation:

$$-\nabla p + \rho \mathbf{g} + \frac{1}{4\pi}(\nabla \times \mathbf{B}) \times \mathbf{B} = 0, \quad (1)$$

where  $\mathbf{g} = -g\hat{\mathbf{z}}$  is the gravitational acceleration,  $p$  is the gas pressure,  $\rho$  is the density, and  $\mathbf{B}$  is the magnetic field. The third term in (1) describes the Lorentz force due to electric currents at the boundary between the flux tube and its local surroundings.

We have developed a numerical code for solving equation (1) in two dimensions; all

quantities are assumed to be independent of the horizontal  $y$  coordinate, so the flux tubes are approximated by sheets. We consider a rectangular domain  $x = [0, L]$  and  $z = [0, H]$ , representing one half of a flux sheet;  $x = 0$  is the flux sheet axis,  $x = L$  is the interface with the neighboring sheet on the right, and  $z = 0$  is the base of the photosphere. The magnetic field is written in terms of a flux function  $A(x, z)$ :

$$B_x = -\frac{\partial A}{\partial z}, \quad B_z = \frac{\partial A}{\partial x}. \quad (2)$$

The boundary conditions are  $A(0, z) = 0$  and  $A(L, z) = A_{\max}$ , where  $A_{\max}$  is one half of the total magnetic flux within the sheet. The gas pressure and density are written as:

$$p = p_{\text{int}}(z) [1 + \beta_0^{-1} F(A)], \quad (3)$$

$$\rho = \rho_{\text{int}}(z) [1 + \beta_0^{-1} F(A)], \quad (4)$$

where  $p_{\text{int}}(z)$  is the internal gas pressure as function of height along the axis of the flux sheet;  $\rho_{\text{int}}(z)$  is the internal density,  $\rho_{\text{int}}(z) = -g^{-1} dp_{\text{int}}/dz$ ;  $\beta_0$  is the ratio of gas- and magnetic pressures at the base (on axis); and  $F(A)$  is a function describing the variation of gas pressure across field lines. Note that the temperature depends only on height ( $p/\rho$  is independent of  $x$ ). The function  $F(A)$  varies from zero on the axis of the sheet to  $F(A_{\max}) = 1$  in the external medium, resulting in distributed electric currents at the interface between the sheet and its local surroundings.

Inserting (2), (3) and (4) into (1) yields

$$\nabla^2 A + 4\pi p_{\text{int}}(z) \beta_0^{-1} \frac{dF}{dA} = 0, \quad (5)$$

which can be solved by minimizing the following Lagrangian:

$$W = \int_0^H \int_0^L \left[ \frac{1}{2} |\nabla A|^2 - 4\pi p_{\text{int}}(z) \beta_0^{-1} F(A) \right] dx dz. \quad (6)$$

The minimization is done by varying the  $A$ -values on a grid of 120 by 240 cells, using the conjugate-gradient method (Press et al. 1992). A similar technique was used in (Hasan et al. 2003), where we constructed a model of a very thin flux tube (see the Appendix of this paper), and in Cranmer & van Ballegoijen (2005). In these papers a Lagrangian description was used, and the radial positions  $r(\Phi, z)$  varied on a fixed grid of  $\Phi$  (the flux function in cylindrical coordinates) and height  $z$ . In the present paper we vary  $A(x, z)$  on a fixed grid of  $x$  and  $z$ .

A model containing one whole flux sheet can be obtained by mirroring the field with respect to  $x = 0$ , and models containing multiple sheets can be obtained by further mirroring

with respect to  $x = L$ . The resulting fields will be used as initial conditions for the two-dimensional MHD calculation (see next subsection).

We perform calculations for a single sheet using the following form for  $F(A)$ :

$$F(A) = \begin{cases} \frac{4}{3}(A/A_{\max})^2 - \frac{1}{3}(A/A_{\max})^8 & \text{if } A \leq A_{\max}, \\ 1 & \text{otherwise.} \end{cases} \quad (7)$$

This produced a smooth transition of gas pressure from the interior to the exterior of the sheet, and the residual magnetic field in the external medium was very small ( $\sim 1$  Gauss). The internal pressure as function of height was approximated as a sum of two exponentials:

$$p_{\text{int}}(z) = p_1 \exp(-z/H_1) + p_2 \exp(-z/H_2), \quad (8)$$

with a photospheric pressure scale height of  $H_1 = 110$  km and a chromospheric scale height of  $H_2 = 220$  km. To obtain kilogauss fields in the photosphere, we used  $\beta_0 = 0.5$ , so that the external gas pressure is three times the internal gas pressure.

In the present calculations we consider a full flux sheet which is placed symmetrically with respect to the midpoint of the computational domain, which we take to be a square of size 1200 km with a uniform grid of  $240 \times 240$  cells, corresponding to a mesh spacing of 5 km in either direction. The axis of the flux tube is now located at  $x = 600$  km. The width of the sheet at  $z = 0$  is approximately 200 km, and the central field strength is 1530 G.

Table 1 provides some of the parameters of the equilibrium model on the tube axis and in the ambient medium at the base ( $z = 0$ ) and the top ( $z = 1200$  km) of the computational domain. Figures 2(a) and (b) depict the variation with height of the temperature and pressure, respectively. It should be noted that the temperature by assumption is constant in the horizontal direction. The sound speed  $c_S$  corresponding to the temperature shown in Figure 2(a) varies from  $7.2 \text{ km s}^{-1}$  at  $z = 0$  to  $9.3 \text{ km s}^{-1}$  at  $z = 1200$  km. In Figure 2(b), the pressure is shown on different field lines corresponding to a fractional flux  $f \equiv A/A_{\max}$  as measured from the left edge of the computational domain. Thus,  $f = 0.5$  corresponds to the tube axis. As expected, the gas pressure on each field line increases as one approaches the tube boundary. The dashed curve ( $f = 0.95$ ) essentially depicts the height variation of the pressure in the ambient medium.

Figures 3(a) and (b) show the height variation of the magnetic field strength  $B$  and of  $\beta$  on various field lines, parameterized, by  $f = 0.5, 0.8, 0.9$ . The field strength on each of the field lines drops rapidly with  $z$  in the first few hundred kilometers after which it approaches a constant value of about 100 G. On the other hand,  $\beta$  is practically constant with  $z$  in the lower region of the atmosphere, which is similar to the behavior one finds in a thin flux tube with equal internal and external temperature at the same height (e.g. see Hasan et al. 2003),



and where both  $B^2$  and  $p$  have the same height dependence. In the upper part of the flux tube,  $B$  is constant and  $\beta$  drops off sharply with  $z$ , essentially mimicking the  $p$  dependence. The Alfvén speed, which is related to  $\beta$  by the approximate relation  $v_A = c_S/\sqrt{\beta}$ , is almost constant (with height) in the lower regions of the atmosphere in the tube, but increases sharply with  $z$  in the higher layers.

Figure 4 shows the variation with horizontal distance  $x$  of the vertical component of the magnetic field  $B_z$  at various heights  $z = 0$  (black solid line), 500 km (black dotted line) and 1000 km (black dashed line). The red curves show the corresponding variation of  $B_x$  measured with respect to the scale on the right. The solid lines (black and red) clearly show that the magnetic field at the base is confined to a width of 200 km. At a height of 1000 km,  $B_x$  becomes very small (a few Gauss) and the field is essentially vertical and constant (approximately 100 G) in the horizontal direction.

### 3. Method and Boundary Conditions

We consider wave generation in the configuration described in the previous section by perturbing the lower boundary and solving the two-dimensional magnetohydrodynamic (MHD) equations in conservation form for an inviscid adiabatic fluid. These consist of the usual continuity, momentum, entropy (without sources) and magnetic induction equations (for details see Steiner, Knölker & Schüssler 1994). The unknown variables are the density, momentum, entropy per unit mass and the magnetic field. We assume that the plasma consists of fully ionized hydrogen with a mean molecular weight of 1.297. The temperature is computed from the specific entropy and the pressure is found using the ideal gas law.

The above MHD equations are solved following the numerical procedure given by Steiner et al. (1994). Briefly, the equations are discretized on a two-dimensional mesh using a finite-volume method which has the advantage of preserving  $\text{div } \mathbf{B} = 0$  to machine accuracy. The method employs finite differences to compute numerical fluxes based on the flux-corrected transport (FCT) scheme of Oran and Boris (1987). The time integration is explicit and has second-order accuracy in the time step. Small time steps are required to satisfy the Courant condition in the upper part of the domain, where the Alfvén speed is large.

Periodic boundary conditions are used at the horizontal boundaries. At the top boundary, (a) the vertical and horizontal components of momentum are set to zero; (b) the density is determined using linear logarithmic extrapolation; (c) the horizontal component of the magnetic field and temperature are set equal to the corresponding values at the preceding interior point. The vertical component of the magnetic field is determined using the con-

dition  $\text{div } B=0$ . Similar conditions are used at the lower boundary, except for the density, temperature and horizontal component of the velocity (or momentum). The density is obtained using cubic spline extrapolation, the temperature is kept constant at its initial value and  $v_x$  at  $z = 0$  is specified as follows:

$$v_x(x, 0, t) = v_0 \sin(2\pi t/P), \quad (9)$$

where  $v_0$  denotes the amplitude of the horizontal motion and  $P$  the wave period. This form was chosen to simulate the effect of transverse motion of the lower boundary. For simplicity, we assume that all points at the lower boundary have this motion, since this does not generate any waves in the ambient medium, other than at the interface with the flux tube, as we shall see later on.

#### 4. Dynamics of a flux sheet

In Sect. 2, we presented a model for a single flux sheet in static equilibrium. The stability of this equilibrium was checked by solving the time-dependent two-dimensional MHD equations without any external driving (assuming rigid boundaries in the vertical direction). We found that this equilibrium was maintained to high accuracy. The maximum amplitude of the flows was no more than a few meters per second over time scales greater than the sound travel time (in both the vertical and horizontal directions), corresponding to over 10000 time steps.

Let us now consider wave generation in the equilibrium atmosphere by means of a transverse motion at the lower boundary ( $z = 0$ ) of the atmosphere, which displaces the flux sheet. We focus on two limiting cases, corresponding to impulsive and periodic excitation, respectively.

##### 4.1. Impulsive excitation

This case corresponds to uniform displacement of the lower boundary at  $z = 0$  to the right which lasts half a wave period ( $P = 240$  s) and then stops. The peak transverse velocity is  $v_0 = 750 \text{ m s}^{-1}$ . Figures 5(a)-(d) show, at times of 52 s, 82 s, 109 s and 136 s, respectively, the velocity field (arrows), the magnetic field (black lines) and the temperature change  $\Delta T = T - T_0$ , where  $T_0$  is the initial temperature at each height. The maximum value of the velocity and the color table for the temperature are shown on the right of each figure. We have omitted velocities smaller than  $30 \text{ m s}^{-1}$ . The white lines denote contours of constant beta for values of  $\beta = 0.1, 0.5, 1.0$  (thick line) and 10.

The horizontal motion of the flux tube at the lower boundary pushes the field lines uniformly to the right. In the flux tube, this motion is communicated to the upper layers as a fast mode, which travels with the local Alfvén speed. The transverse motion of the field lines compresses the gas on the right interface of the tube and the ambient medium (above the base, where there is no horizontal motion in the field free medium).

Figure 6 clearly shows at  $t = 82$  s the development of a pressure enhancement and depletion, respectively, at the right and left interfaces of the tube with respect to the field free gas. This essentially creates a pressure dipole which in turn generates a vortex motion with upflow and downflow motions on the right and left sides, respectively. The top of the vortex motion is in the opposite direction to that at the base. From Figure 5 we find that, as time proceeds, the vortex grows in size and also moves upward. This motion carries the field lines, pushing them slightly counterclockwise in the lower regions of atmosphere.

As the vortex extends upwards, there is a hint of a shock forming at its upper edge, as can be seen in Figure 5(c). Once the transverse driving motion stops at the base, the vortex motions diminish and the flow is now guided along the field lines. This is evident in Figure 5(d) which shows at  $t = 136$  s negligible flows near the base of the flux tube and large flows almost aligned with the magnetic field in the upper atmosphere. The large upflows generate a shock which can be discerned at a height of about 900 km along with a temperature enhancement greater than 400 K.

Figures 7(a) and (b) denote the  $z$  variation of  $v_s$  and  $v_n$ , the field-aligned and normal velocity components respectively at the times of 82, 109 and 150 s along a specific field line. We choose a field line parameterized by  $f = 0.6$ , which is just to the right of the flux tube axis. Let us first consider the behavior of the field-aligned flow, shown in Figure 7(a). As time proceeds, the vertical component of the velocity pulse increases with height in magnitude on account of the density stratification and it steepens on account of nonlinear effects as it propagates upward. At  $t = 150$  s the pulse resembles a shock. The presence of a wake behind the shock should also be noted, which is a generic feature associated with the propagation of a pulse in a vertically stratified atmosphere (e.g. Hasan et al. 2003). Figure 7(b) shows the  $z$  variation of the normal component of the flow. The curves corresponding to  $t = 82$  and 109 s show the normal component profiles during the impulsive phase (i.e., during the interval of transverse driving motion at the base is present). The dashed curve shows the profile at  $t = 150$  s, after the transverse motion at the base has halted. This profile is broadened due to the fact that the Alfvén speed, which is the characteristic propagation speed of the transverse pulse, increases sharply with height. In the lower regions of the atmosphere, where  $\beta \approx 0.6$ ,  $v_A \approx 10 \text{ km s}^{-1}$ , whereas at a height of 600 km, it has increased to about  $26 \text{ km s}^{-1}$ .

## 4.2. Periodic excitation

We now consider the periodic excitation of waves due to transverse driving of the lower boundary, with a period of 24 s (similar to Rosenthal et al. and Bogdan et al.), though with a higher amplitude of  $750 \text{ m s}^{-1}$ . Figures 8(a)-(d) show the wave pattern that develops in this case. As before, the colors are used to denote the temperature perturbation with respect to the initial value at each height and the white curves depict contours of constant  $\beta$ .

The horizontal motion of the tube at the lower boundary is a source of acoustic waves just outside the flux tube boundary in the ambient medium, in which they propagate isotropically and near the interface as ‘spherical’ acoustic waves. The yellow and blue strips associated with  $\Delta T$ , with an almost constant separation, clearly show the acoustic waves propagating outwards at the sound speed from their source near the bottom edge of the tube. The wavelength of these waves is approximately constant since the acoustic speed varies weakly in the lower part of the computational domain.

In the flux tube, the horizontal driving motions generate both fast and slow modes. Close to the tube axis, the field is strong ( $\beta < 1$ ) and the transverse motion generates a fast mode which propagates upwards at the Alfvén speed. Its propagation can be clearly seen in Figure 9, which depicts the variation of the normal velocity component  $v_n$  as a color contour plot. The fast wave front shows an asymmetry in propagation since the Alfvén speed is largest on the tube axis and decreases in the horizontal direction. The increase in separation in the vertical direction between the color peaks clearly shows the increase in wavelength due to the increase in Alfvén speed with  $z$ , which increases very rapidly with height from about  $10 \text{ km s}^{-1}$  at the base to about  $100 \text{ km s}^{-1}$  at the top of our computational box.

The horizontal motions in the central part of the flux tube produce compressions and decompressions of the gas at the edge of the tube, where the magnetic field is weaker ( $\beta \gtrsim 1$ ). The resulting pressure variations are periodic in height and time, and are  $180^\circ$  out of phase on the two sides of the flux tube. The associated pressure gradients drive periodic vertical flows that propagate upward along the edge of the flux tube at the speed of the transverse wave. These vertical flows are an integral part of the flux tube wave, so the wave has both transverse and longitudinal character in different parts of the tube. As the wave travels upward, it reaches a height where the magnetic field at the edge of the tube becomes more horizontal, and longitudinal motions are driven into the central part of the flux tube where  $\beta < 1$ ; this process is analogous to the mode conversion discussed by Bogdan et al. (2003). In the low- $\beta$  region, the wave consists of two almost decoupled parts: a fast mode that propagates in all directions, described in the preceding paragraph (see Figure 9), and two slow modes that are guided along the field lines. The slow modes on opposite sides of tube axis are  $180^\circ$  out of phase with each other, and their amplitudes increase with height due to

the stratification. Being mainly acoustic in nature, they produce a compression and heating of the plasma in the chromosphere. This can be discerned for instance in Figure 8(d), where the wave front located at a height of about a 1000 km produces heating greater than 500 K. Figure 10 shows the variation of the field-aligned velocity component,  $v_s$ , on a field line  $f = 0.6$  at three different times, shown by the different curves. One can see the amplitude increase and steepening of the wave due to nonlinear effects as it propagates upward at the acoustic speed of around  $8 \text{ km s}^{-1}$ . This clearly establishes the nature of this wave to be acoustic. It is interesting to note the occurrence of weak shocks at a Mach number of about 0.2.

## 5. Discussion and Summary

The present investigation is a continuation of our earlier work on the dynamics of the magnetic network on the Sun. In our previous studies we used a simplified picture of magnetic elements in terms of a quasi one-dimensional treatment based on the thin flux tube approximation. This approach was useful in providing a qualitative picture of wave propagation and nonlinear mode coupling in the lower regions of the atmosphere where the thin flux tube approximation is applicable. However, as already pointed out in Sect. 1, this approximation breaks down in the chromosphere due to the expansion of the flux tube with height as well as due to the merging of different tubes. We overcome these limitations by using a two-dimensional treatment. In the first part of this study we focus on a single flux tube and examine the consequences when the lower boundary is perturbed by a transverse motion. Future work will extend the present analysis to multiple tubes as well as other types of excitation mechanisms.

The choice of using a transverse velocity perturbation at the lower boundary was to some extent motivated by observations, particularly those of Muller and Rodier (1992) and Muller et al. (1994) who studied the footpoint motions of a large number of network bright points, generally regarded as a proxy for magnetic elements. We considered the driving motions to occur at a fixed height in the atmosphere. In reality, we expect that the displacement of the flux tubes occurs in response to turbulent motions below the photospheric base. These flows are absent or weak on the surface. Thus, the pressure fluctuations in our model are a direct consequence of the relative motion of the flux tube with respect to its local surroundings. These play a key role in driving the vortex motions that propagate high up in the flux tube. It appears reasonable to expect that such pressure fluctuations indeed occur in the solar network.

We chose two limiting forms for the time behavior of the perturbation as an idealization

for drivers that (a) generate discrete pulses well separated in time and, (b) are periodic and continuous. The values of the time constant for the pulse in the first case and the wave period in the second case were chosen because of practical considerations related to the limit of not letting the simulation exceed a total time where reflections from the top boundary become important.

We find that the transverse driving motions at the lower boundary lead to strong pressure perturbations in the field-free medium at the tube interface. This is an efficient process for generating vortical motions, recognized earlier by Shibata (1983) in two-dimensional simulations, who found that such motions can arise due to a pressure perturbation applied at the base of a uniformly magnetized stratified atmosphere ( $\beta > 1$ ). In our simulations the strong pressure fluctuations are essentially localized in regions where  $\beta$  is greater than unity. The observational signature associated with vortex formation would be the prediction of simultaneous upward and downward motions on opposite sides of flux tubes. Under what conditions does a vortex form? It appears that for wave periods that are sufficiently long (compared to the Alfvén travel time) the dynamics is likely to be dominated by vortical motions, but it is difficult at this stage to say anything more definitive.

An important consequence of our calculations is that the interface between the flux tube and the ambient medium is both a source of acoustic waves in the ambient medium as well as fast and slow waves just inside the flux tube. This can have interesting consequences: the acoustic waves that travel isotropically in the field free medium will impinge on neighboring flux tubes in the network and excite waves in them. On the other hand the modes generated in the high  $\beta$  region of the tube (at the interface) undergo mode conversion as they propagate upward and enter the region where  $\beta \approx 1$ , as also found by Rosenthal et al. (2002) and Bogdan et al. (2003). In the upper part of the flux tube where the field is essentially vertical and  $\beta \ll 1$ , the acoustic-like longitudinal motions steepen and form shocks accompanied by heating, as also found out for instance by Hasan & Ulmschneider (2004) using a thin flux tube calculation. There is, however, an important qualitative difference between the present results and those of Zhugzhda et al. 1995, Hasan et al. (2003) and Hasan & Ulmschneider (2004). In the latter, longitudinal motions are generated from transverse driving motions at the flux tube footpoints as a consequence of nonlinear mode coupling that is most efficient when the transverse and longitudinal mode speeds are comparable (roughly for  $\beta \approx 0.2$ ). In the present work, the mode conversion occurs essentially in the linear regime and is a consequence of the spatial variation of  $\beta$  in the tube. We find that transverse driving motions with velocities less than  $1 \text{ km s}^{-1}$  are sufficient to produce strong shocks in the chromosphere.

The present work is in the spirit of the investigations by Rosenthal et al. (2002) and

Bogdan et al. (2003) on wave propagation in two-dimensional magnetic structures. There are, however, qualitative differences between the initial state and the form of the perturbation used for driving the atmosphere in the two sets of calculations. For instance, the initial equilibrium configuration adopted by the above authors assumes a potential field that is typical of the large-scale pattern connecting different network regions. Bogdan et al. (2003) consider a unipolar magnetic structure which at the base is 2000 km wide surrounded by smaller magnetized regions (about 750 km wide) of opposite polarity (as shown in Figure 1 of their paper). At larger horizontal distance from the flux concentration, the field is essentially horizontal though much weaker. Thus, in the above configuration the entire atmosphere is magnetized. On the other hand, we consider a discrete unipolar vertical flux, with a transverse dimension of about 200 km, in magnetostatic equilibrium (and non-potential field). Our equilibrium model, possessing a sharp interface between the tube and the ambient field-free medium, is perhaps more representative of a flux element in the solar network. A minor difference is that the atmosphere in our model is not isothermal in the vertical direction but has a temperature increase with height similar to that in the solar chromosphere.

Secondly, in our model, the whole flux tube at the photosphere is displaced and not just a small region inside it. The driving motion in the simulations of Bogdan et al. (2003) is confined to a region about 400 km wide within the flux element. In our simulations, the transverse motion of the entire magnetic element creates strong pressure perturbations just outside the tube which in turn are responsible for the vortical motions and the generation of acoustic waves in the ambient medium as well as the strong longitudinal motions that eventually produce shock heating in the upper atmosphere. The recognition that the flux tube interface is a source of acoustic waves in the ambient medium and that these waves can penetrate back into the tube at higher elevations is a new feature of the present work. Thirdly, in addition to periodic driving, we also consider impulsive motions at the lower boundary.

We should point out some limitations of our current study. Our analysis is based on a two-dimensional treatment in slab geometry, assuming that fluid displacements are confined to the  $x - z$  plane. The waves examined by us are different from the kink and sausage modes treated earlier by us using a simplified thin flux tube approximation. Ideally, one would use a 3-D treatment which is presently beyond the scope of this work. Our analysis also neglects the torsional Alfvén wave, which in reality would couple to the fast and slow modes. Even within the two-dimensional framework, we have had to restrict the height range in our simulations to 1200 km, since the Alfvén speed (that essentially controls the time step used in the numerical scheme) increases very rapidly with  $z$ .

In summary this paper is the first of a series of investigations on the dynamics of the solar magnetic network based on a two-dimensional treatment of the MHD equations. We have made a start by considering processes occurring in a single flux tube which expands with height in the photosphere and assumes a "wine glass" geometry in the chromosphere. Flows and wave motions are generated in this configuration by transverse motions at the base of the flux tube. For impulsive driving we find the presence of vortical motions. An interesting feature for both impulsive and periodic driving, is the development of shock-like features in the upper atmosphere which can be important in heating the chromosphere. We hope to extend the scope of the present calculation in future work to include multiple flux tubes as well as include a larger height extension in order to estimate transport of energy in to the corona through this mechanism.

SSH thankfully acknowledges support from the National Science Foundation, U.S.A. through grant number ATM-0207641.

## REFERENCES

- Bogdan, T. J., Carlsson, M. Hansteen, V., McMurry, A., Rosenthal, C. S., Johnson, M., Petty-Powell, S., Zita, E. J., Stein, R. F., McIntosh, S. W., & Nordlund, Å 2003, ApJ, 599, 626
- Cargill, P. J., Spicer, D. S., & Zalesak, S. T. 1997, ApJ, 488, 854
- Carlsson, M., & Stein, R. F. 1995, ApJ, 440, L29
- Choudhuri, A. R., Auffret, H., & Priest, E. R. 1993, Sol. Phys., 143, 49
- Cranmer, S. R., & van Ballegoijen, A. A. 2005, ApJ Suppl., 156, 265
- Curdt, W., & Heinzel, P. 1998, ApJ, 503, L95
- Fawzy D., Rammacher W., Ulmschneider P., Musielak Z.E., Stępień K., 2002, A&A, 386, 971
- Grossmann-Doerth, U., Kneer, F., & v. Uexküll, M. 1974, Sol. Phys., 37, 85
- Hasan, S. S., & Kalkofen, W. 1999, ApJ, 519, 899
- Hasan, S. S., Kalkofen, W., & van Ballegoijen, A. A. 2000, ApJ, 535, L67



- Hasan, S. S., Kalkofen, W., van Ballegooijen, A. A., & Ulmschneider, P. 2003, *ApJ*, 585, 1138
- Hasan, S. S., & Ulmschneider, P. 2004, *A & A*, 422, 1085
- Hollweg, J. V., Jackson, S., & Galloway, D. 1982, *Sol. Phys.*, 75, 35
- Huang, P., Musielak, Z. E., & Ulmschneider, P. 1995, *A & A*, 297, 579
- Kalkofen, W. 1997, *ApJ*, 486, L148
- Lites, B. W., Rutten, R. J., & Kalkofen, W. 1993, *ApJ*, 414, 345
- McAteer, R. T. J., Gallagher, P. T., Williams, D. R., Mathioudakis, M., Phillips, K. J. H. & Keenan, F. P. 2002, *ApJ*, 567, L168
- McAteer, R. T. J., Gallagher, P. T., Williams, D. R., et al. 2003, *ApJ*, 587, 806
- Muller, R., & Roudier, Th. 1992, *Sol. Phys.*, 141, 27
- Muller, R., Roudier, Th., Vigneau, J., & Auffret, H. 1994, *A & A*, 283, 232 *ApJ*, 448, 865
- Noble, M. W., Musielak, Z. E & Ulmschneider, P. 1998, *A & A*, 409, 1085
- Ofman, L. & Davila, J. M. 1998, *J. Geophys. Res.*, 103, 23.677
- Ofman, L., Nakariakov, V. M., & DeForest, C. E. 1999, *ApJ*, 514, 441
- Oran, E. S., & Boris, J. P. 1987, *Numerical Simulations of Reactive Flow* (New York: Elsevier)
- Rosenthal, C. S., Bogdan, T. J., Carlsson, M., Dorch, S. B. F., Hansteen, V., McIntosh, S. W., McMurry, A., Nordlund, Å& Stein, R. F. 2002, *ApJ*, 564, 508
- Rutten, R. J. & Uitenbroek, H. 1991, *Sol. Phys.*, 134, 15
- Sakai, J. I., Igarshi, J. & Kawata, T. 1998, *Sol. Phys.*, 181, 13
- Shibata, K. 1983, *PASJ*, 35, 263
- Skumanich, A., Smythe, C. & Frazier, E. N. *ApJ*, 200, 747
- Spruit, H. C. 1981, *A & A*, 102, 129
- Steiner, O., Knölker, M. & Schüssler, M. 1994, in *Solar Surface Magnetism*, ed. R. J. Rutten & C. J. Schrijver (NATO ASI Ser. C-433) (Dordrecht: Kluwer), p. 441

Ulmschneider, P. 2003, in Lectures on Solar Physics, Antia H.M., Bhatnagar A., Ulmschneider P., Eds., Lecture Notes in Physics 619, Springer Verlag, Heidelberg, Berlin, p. 232

Ulmschneider, P., Zähringer, K., & Musielak, Z. E. 1991, A & A, 241, 625

von Uexküll, M., & Kneer, F. 1995, A & A, 294, 252

Zhugzhda, Y. D., Bromm, V., & Ulmschneider, P. 1995, A & A, 300, 302

Table 1. Parameters on the Tube Axis & Ambient Medium

Variable	Tube Axis		Ambient Medium	
	Base	Top	Base	Top
Temperature	4800 K	8200 K	4800 K	8200 K
Density	$1.3 \cdot 10^{-7} \text{ g cm}^{-3}$	$9.5 \cdot 10^{-12} \text{ g cm}^{-3}$	$4.0 \cdot 10^{-7} \text{ g cm}^{-3}$	$2.9 \cdot 10^{-11} \text{ g cm}^{-3}$
Pressure	$4.1 \cdot 10^4 \text{ dyn cm}^{-2}$	$8.3 \text{ dyn cm}^{-2}$	$1.2 \cdot 10^5 \text{ dyn cm}^{-2}$	$22 \text{ dyn cm}^{-2}$
Sound speed	$7.1 \text{ km s}^{-1}$	$9.3 \text{ km s}^{-1}$	$7.1 \text{ km s}^{-1}$	$9.3 \text{ km s}^{-1}$
Alfvén speed	$11 \text{ km s}^{-1}$	$93 \text{ km s}^{-1}$	...	...
Magnetic field	1420 G	102 G	...	...
$\beta$	0.5	0.02	...	...

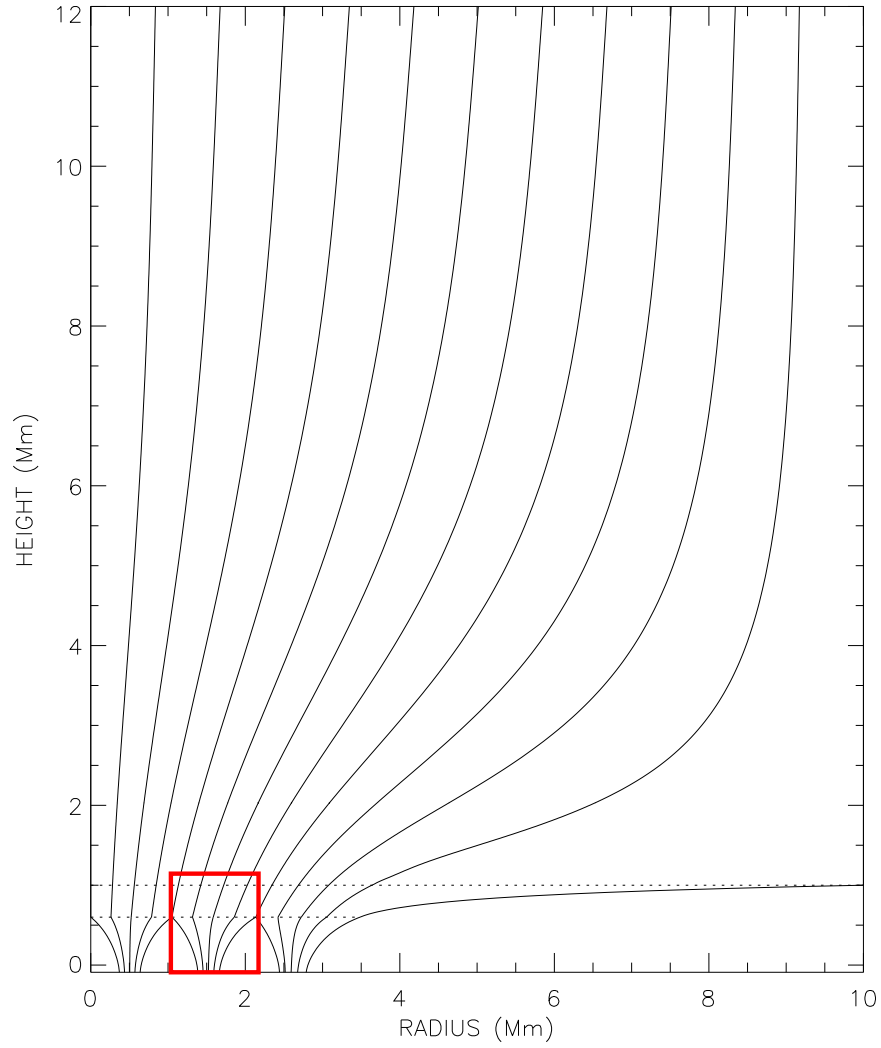


Fig. 1.— Model of a network element consisting of individual flux tubes separated at the photospheric surface by a distance of 1000 km which merge at a height of about 600 km. The red box corresponds to the domain taken up for dynamical simulations.

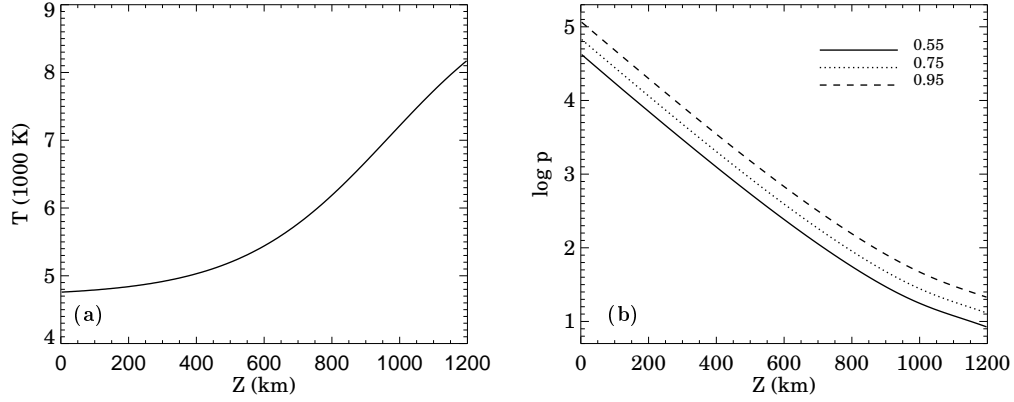


Fig. 2.— Variation of (a) the temperature  $T$ , and (b) the logarithm of the pressure  $p$  as a function of height on the field lines corresponding to  $f = 0.55$  (solid curve), 0.75 (dotted curve) and 0.95 (dashed curve) in the equilibrium configuration. Note the temperature is uniform (by assumption) in the horizontal direction.

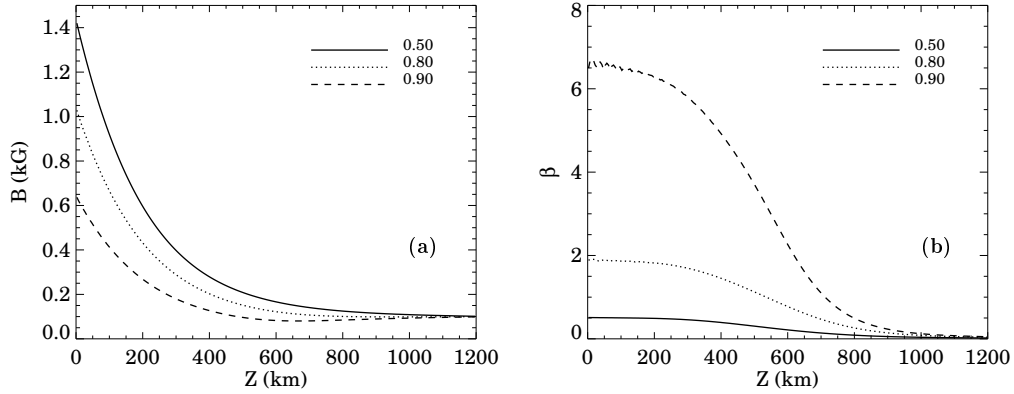


Fig. 3.— Variation of (a) the magnetic field strength  $B$ , and (b)  $\beta$  as a function of height on the field lines corresponding to  $f = 0.5$  (solid curve), 0.8 (dotted curve) and 0.9 (dashed curve) in the equilibrium configuration.

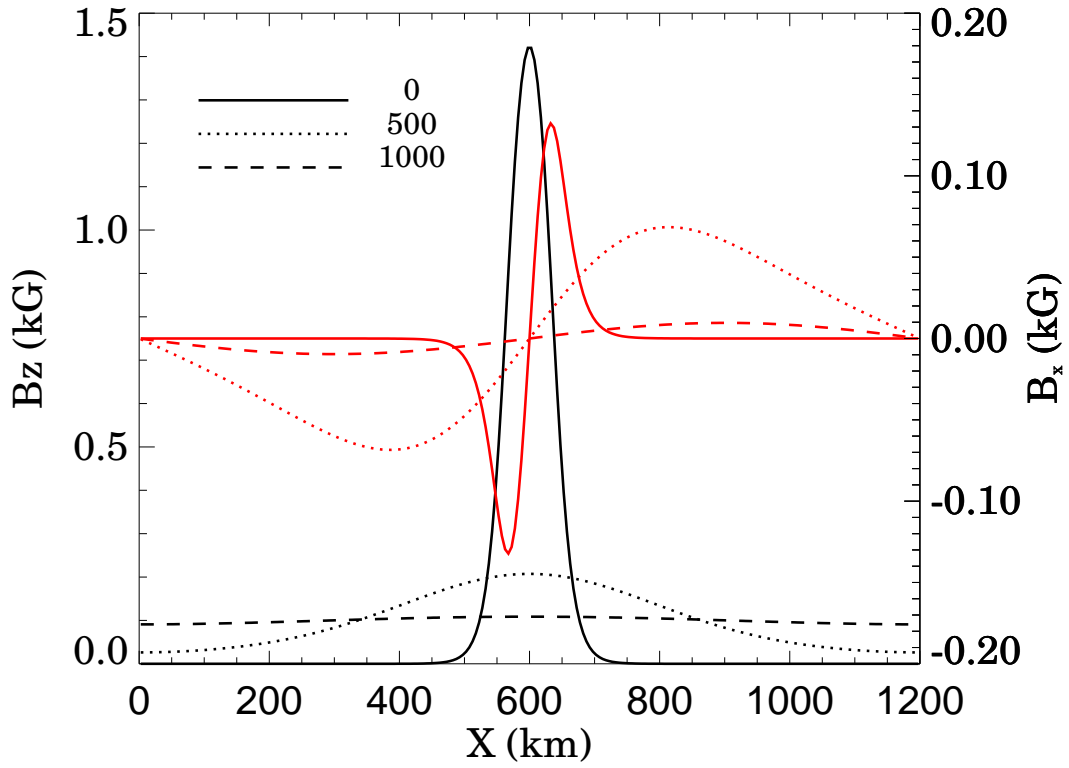


Fig. 4.— Variation of  $B_z$  with horizontal distance (from the left edge of the computational domain) at the following heights:  $z = 0$  (black solid line), 500 km (black dotted line) and 1000 km (black dashed line). The corresponding red curves denote  $B_x$  measured with respect to the values given on the right scale.

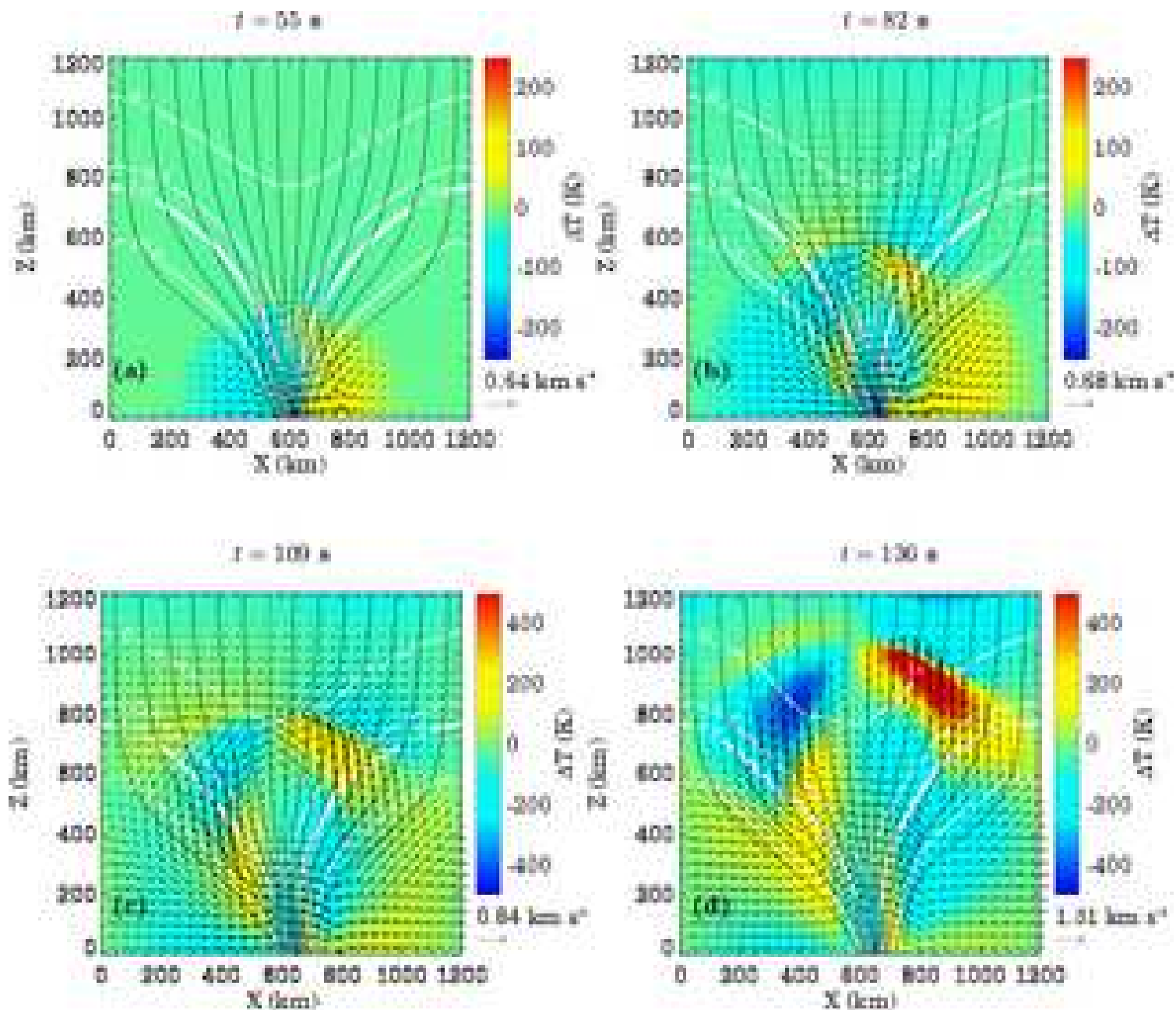


Fig. 5.— Flow pattern and temperature perturbation,  $\Delta T$ , (about the initial state) at (a) 55 s, (b) 82 s, (c) 109 s and (d) 136 s in a network element due to horizontal motion at the lower boundary, with an amplitude of  $750 \text{ m s}^{-1}$ , applied for half a wave period ( $P = 240$  s), after which the motion ceases. The thin black curves are the magnetic field lines, the arrows denote the direction of the flow, and the color scale shows the temperature perturbation. The white curves denote contours of constant  $\beta$  corresponding to  $\beta = 0.1, 0.5, 1.0$  (thick curve) and 10.

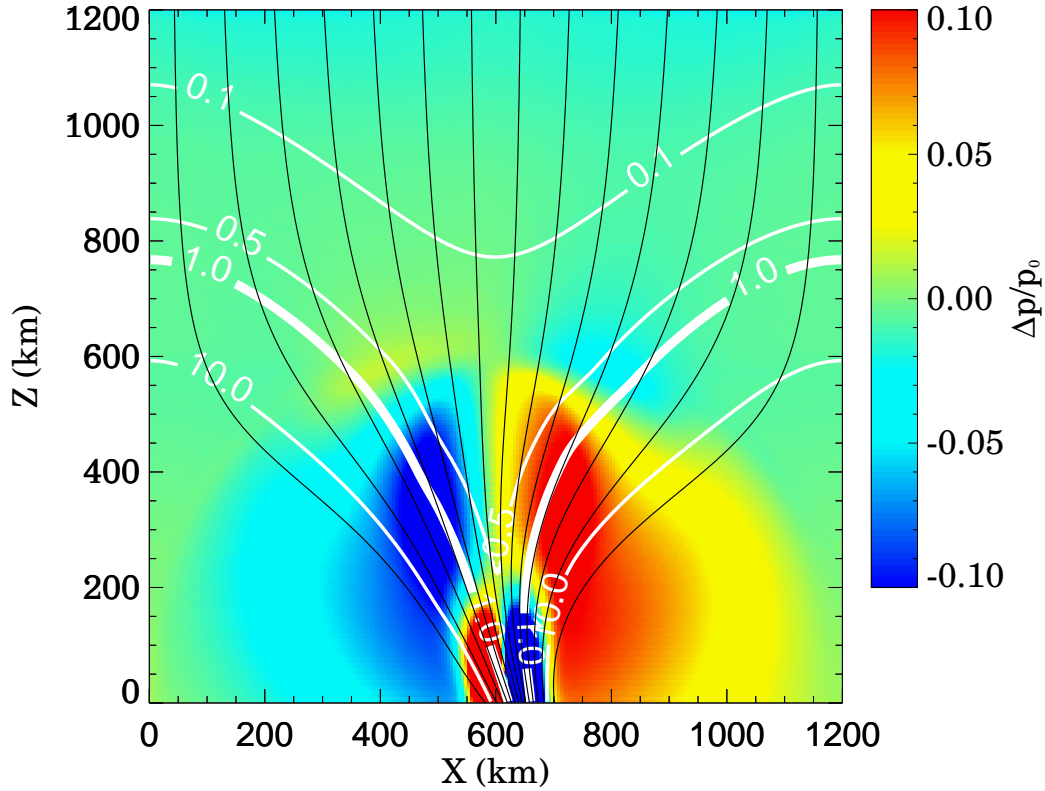


Fig. 6.— The relative pressure perturbation (about the initial state),  $\Delta p/p_0$ , at  $t = 82$  s in a network element due to horizontal motion at the lower boundary with an amplitude of  $750 \text{ m s}^{-1}$  and a period of  $P = 240$  s. The thin black curves are the magnetic field lines and the white curves denote contours of constant  $\beta$  corresponding to  $\beta = 0.1, 0.5, 1.0$  (thick curve) and  $10$ .



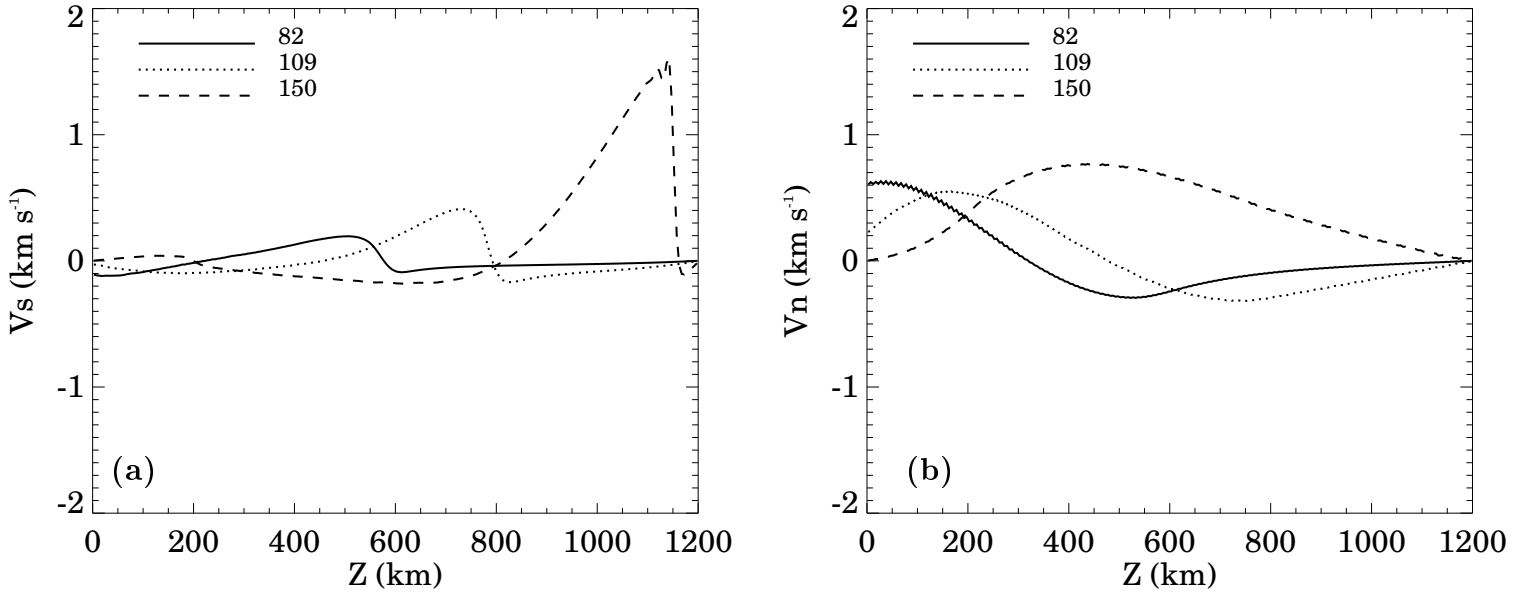


Fig. 7.— Variation of the velocity components (a) along the magnetic field  $v_s$  and (b) normal to the magnetic field  $v_n$  at different  $t = 82$  s (solid curve), 109 s (dotted curve) and 150 s (dashed curve) on a field line characterized by  $f = 0.6$  in a network element due to a horizontal motion at the lower boundary with an amplitude of  $750 \text{ m s}^{-1}$  and a period  $P = 240$  s.

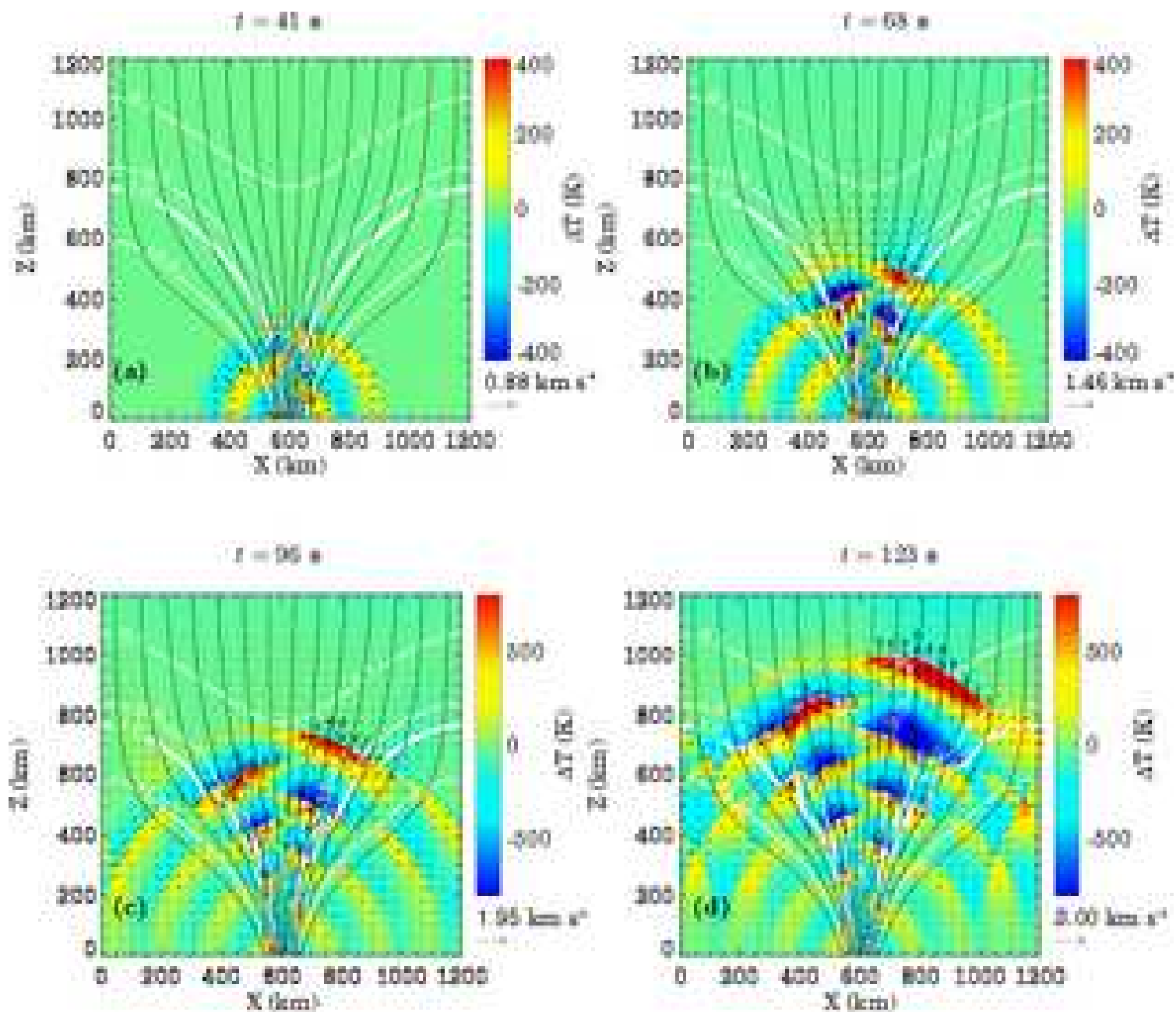


Fig. 8.— Flow pattern (arrows) and the temperature perturbation (about the initial state),  $\Delta T$ , at (a) 41 s, (b) 68 s, (c) 96 s and (d) 123 s in a network element due to a periodic horizontal motion at the lower boundary with an amplitude of  $750 \text{ m s}^{-1}$  and a wave period of  $P = 24$  s. The thin black curves are the magnetic field lines. The white curves denote contours of constant  $\beta$  corresponding to  $\beta = 0.1, 0.5, 1.0$  (thick curve) and 10.

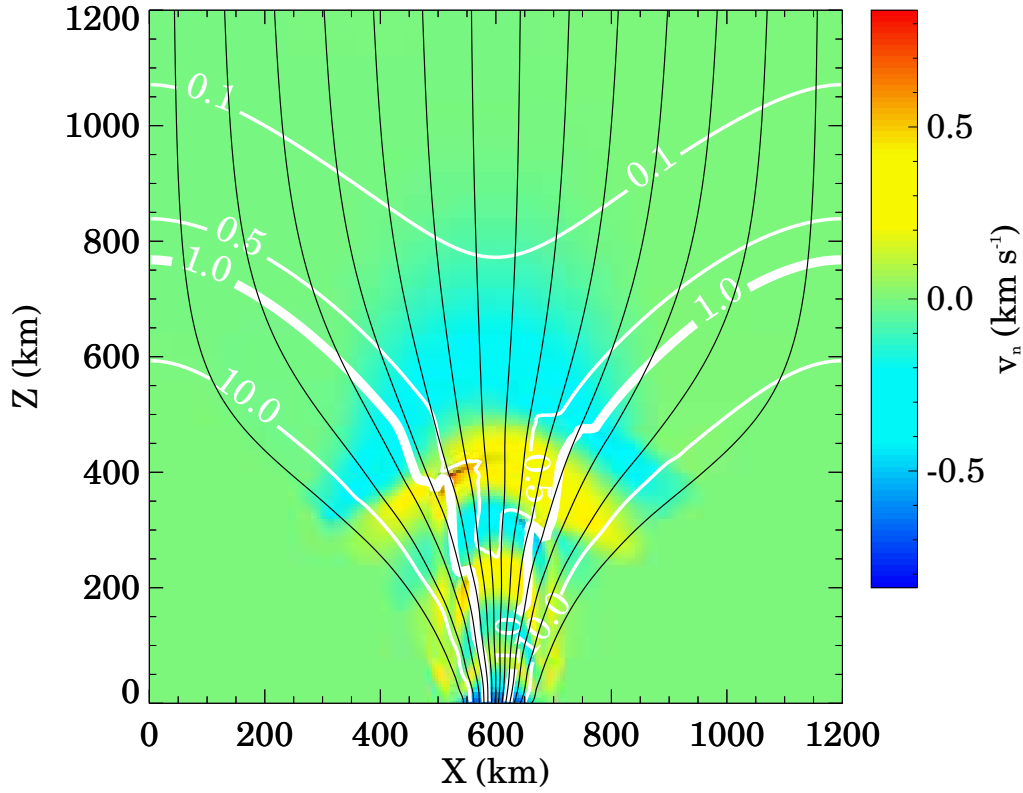


Fig. 9.— The normal velocity component  $v_n$  at  $t = 68$  s in a network element due to a horizontal motion at the lower boundary with an amplitude of  $750 \text{ m s}^{-1}$  and a period of  $P = 24$  s. The thin black curves are the magnetic field lines and the white curves denote contours of constant  $\beta$ , corresponding to  $\beta = 0.1, 0.5, 1.0$  (thick curve) and  $10$ .

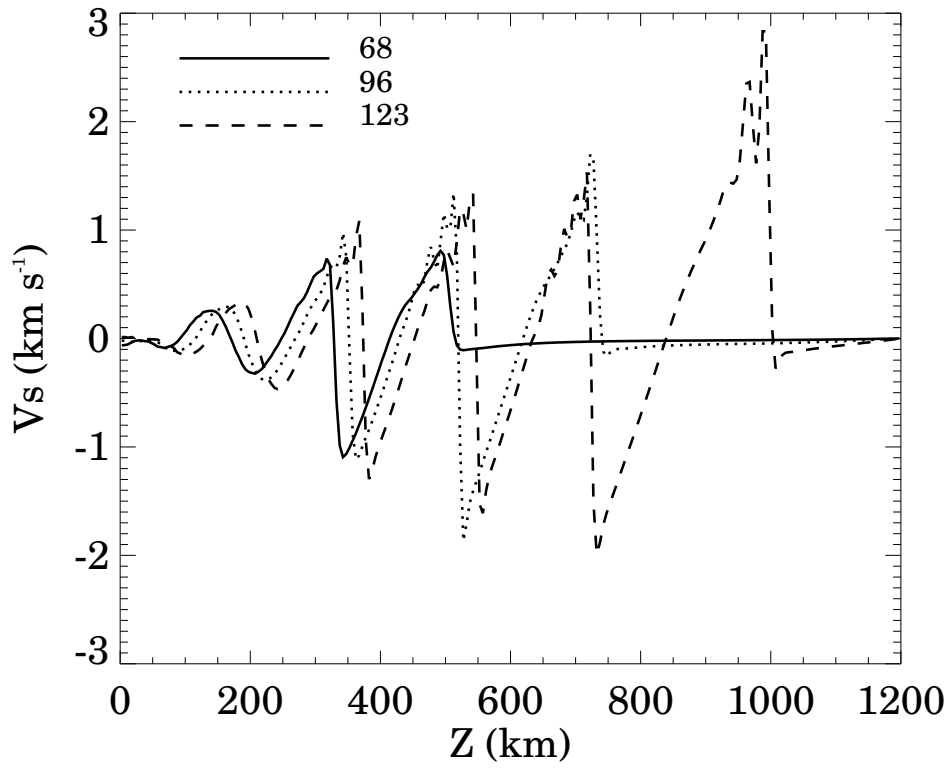


Fig. 10.— Variation of the velocity component along the magnetic field,  $v_s$ , at times  $t = 68$  s (solid curve), 96 s (dotted curve) and 123 s (dashed curve) on a field line characterized by  $f = 0.6$  in a network element due to horizontal motion at the lower boundary with an amplitude of  $750 \text{ m s}^{-1}$  and a period of  $P = 240$  s.